Proceedings of the 13th
Mediterranean Conference on Control and Automation
Limassol, Cyprus, June 27-29, 2005

TuA03-3

Endpoint-Side Optimization of a Five Degree-of-Freedom Haptic Mechanism

Kostas Vlachos, and Evangelos Papadopoulos, *Senior Member, IEEE*

Abstract—One of the main issues in the design of haptic devices is to provide maximum transparency. In this paper a design methodology, which aims at the maximization of the transparency for a low-force five degree-of-freedom (dof) haptic device, is presented. The haptic device is optimized along a typical path with proper tolerances, rather than at some workspace operating point. The device, part of a training medical simulator for urological operations, consists of a two dof, 5-bar linkage and a three dof spherical joint. The requirement for reliable reproduction of low torques and forces leads to the need for maximum transparency, in other words to the need for minimization of device induced parasitic forces and torques. The multivariable optimization employed is based on the minimization of an objective function that includes all the haptic device mass/inertia properties as seen from the user side. Kinematical and operational constraints are taken into account. A new 5-dof haptic mechanism is constructed according to the optimization results. The optimized mechanism is substantially improved with respect to an existing device.

I. INTRODUCTION

THE use of simulators is now an accepted tool in the training of surgeons [1]. Although it is still early for definitive conclusions, it seems that there are many advantages in the use of simulators. Simulator-based training is less expensive and results in efficient and customizable training in complex operations [2]. Training on patients can result in serious damages and lawsuits while training on animals becomes an undesirable alternative for ethical and economical reasons. Furthermore the anatomy of an animal is not always close enough to that of the human. Also, the existence of a training simulator increases the availability of the training environment, allows an easier evaluation of the performance of the trainee, and can be used to introduce various operation scenarios or situations.

Realistic medical simulators consist of a graphical environment, which reproduces the visual information that the surgeon obtains during an operation, a haptic device, which is responsible for haptic data interchange (forces and torques), and positions and orientations interchange between user and the virtual environment, and a control system, which coordinates and controls the graphical environment and the haptic device. Today, one can distinguish two trends in the development of medical simulators. The first is characterized by the use of general-purpose haptic devices, like the Phantom or the Freedom-7 [3]-[5]. The second trend is characterized by the use of haptic devices designed for a specific operation [6]-[9].

The faithful reproduction of the real forces and torques that the surgeon feels during an operation is of great importance. Therefore, the mechanism should be as transparent as possible. By transparency it is understood that the user of the haptic mechanism should feel nothing else but the appropriate forces/torques. In order to achieve this, the haptic mechanism must be designed so that its effects do not show up, i.e., with minimum mass matrix, $\tilde{\mathbf{M}}$, minimum gravity vector $\tilde{\mathbf{G}}$, and minimum vector of nonlinear velocity terms $\tilde{\mathbf{V}}$ as seen from the user side.

Optimization techniques have been already used in improving the performance of mechanisms and manipulators. The inertial and acceleration characteristics of manipulators have been discussed in [10]. Optimization techniques are used to determine the smallest inertial properties and the maximum achievable acceleration of the end-effector in every direction over the workspace. A global isotropy index has been proposed to quantify a configuration independent isotropy of a robot's Jacobian or mass matrix [11]. This index was used to compare the performance of three manipulators, including two parallel platform robots and a hybrid robot [12]. A two-dof haptic device was optimized with respect to workspace, intrusion, inertia, response and structural properties [13]. The architecture of a parallel redundant mechanism has been optimized from a kinematical viewpoint [14]. The dexterity, uniformity and actuator forces have been investigated as potential objective functions. Authors' previous work has presented the design of a five-dof haptic interface, which was partly optimized with respect to its condition number and perceived inertia under several kinematical constraints [9]. The same haptic device is further optimized in [16] using multi-objective optimization based on the minimization of two objective

functions that include mass/inertia properties and joint friction.

This paper presents a multivariable optimization methodology resulting in a low-force five-bar haptic device with maximized transparency, using an objective function and minimizing not only specific mass/inertia properties, but all the haptic device mass/inertia properties as seen from the user side.

The objective function consists of the mass/inertia parts that appear in the Langrage equation of motion of the haptic device as seen from the user. The optimal design is achieved for a typical endoscope path, allowing at the same time small deviations from it. The methodology results in a) optimum mechanism geometry, b) optimum location of the endoscope path end point with respect to the haptic device base, c) optimum balancing weights, d) optimum location of the balancing weights, e) optimum motors for the 5-bar mechanism, and f) optimum transmission ratio between the 5-bar mechanism motors and links. The proposed optimization methodology is suitable for any mechanism that should be optimized along a given path, with or without kinematical and operational constraints. The paper describes in detail the objective function employed, the optimization constraints and the overall procedure. Finally, optimization results and the, according to these results, constructed haptic device are presented.

II. Description of the Haptic Device

As mentioned above, the haptic device is used in a training simulator for urological operations. During a urological operation on a male patient, the surgeon inserts a long cylindrical endoscope until its endpoint reaches the patient's bladder. During insertion, the endoscope follows a path such as the typical one shown in Fig. 1. The surgeon moves the tip of the endoscope from the insertion point A to the final point C, via an intermediate point B, see Fig. 1. At point B, the endoscope orientation changes without translation, so as to align the entire urethra and continue the insertion phase without traumas. The corresponding endoscope configurations labeled by a, b, c, d, are shown in Fig. 1.

When the tip of the endoscope reaches the bladder (point C in Fig. 1), the surgeon inserts through the endoscope a mechanism with a scissor-like handle and begins the second phase. This phase is the main operation in which tissue removal occurs. During this phase, the movements of the endoscope are mainly rotational. Observations during our previous work showed that a haptic mechanism with two translational and three rotational dof is needed, [9]. The actual kinematical requirements that define the minimum workspace of the haptic interface were found by observations of typical urological operations. These resulted in a tool displacement requirement along the X and Y axes equal to 0.1 m, while rotation requirements around the X′ is ±180° and around the Z′ and Y′ is ±30°.
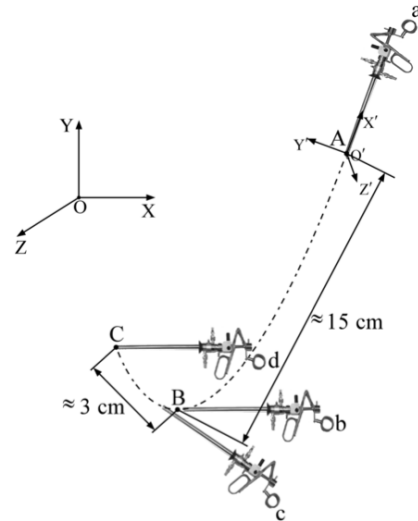

Fig. 1. Endoscope endpoint path and orientation during an operation.

The first prototype consists of a two dof, 5-bar linkage and a three dof spherical joint. To reduce mechanism moving mass and inertia, all actuators are placed at the base. The transmission system is implemented using tendon drives with capstans. In the first version of the haptic device [9] the link lengths, l_1, l_2, l_3, l_4, of the five-bar mechanism were optimized in order to minimize the condition number of the mechanism along a path, under kinematical and structural constraints. The path was fixed in space relative to the mechanism base.

A second optimization procedure is presented in [16], where a multiobjective optimization methodology is used. Two objective functions are defined, the first focusing at mass/inertia optimization and the second at joint friction.

The methodology results in optimum mechanism geometry, l_1, l_2, l_3, l_4, and optimum location of the endoscope path end point, C_x, C_y, with respect to the haptic device base. Table I presents the results.

TABLE I
OPTIMIZATION RESULTS

Optimized variables	Value
Length of link 1, l_1	0.110 m
Length of link 2, l_2	0.060 m
Length of link 3, l_3	0.110 m
Length of link 4, l_4	0.170 m
X coordinate of point C, C_x	0.064 m
Y coordinate of point C, C_y	-0.126 m

III. New Optimization Design

An exact optimization of the mechanism transparency would require the minimization of the device induced parasitic forces and torques as seen from the user side. Therefore the problem that we present here is much more complex. Our goal is not to minimize the condition number

of the mechanism along a path, as in [9], or mass/inertia and friction along the same path, as in [16], under kinematical and structural constraints, but to design a haptic device with maximum transparency under kinematical and structural constraints.

The optimization goal is to find the main *mechanism design parameters and configuration*, so that the device *transparency is maximized*. The unknown design parameters are a) the dimensions of the 5-bar linkage and the spherical joint, b) the location of the typical path ABC relative to the mechanism base, c) optimum balancing weights, d) optimum location of the balancing weights, and e) optimum transmission ratio between the 5-bar mechanism motors and links (see Fig. 2). In order to define the unknown parameters we make the following assumptions and observations.
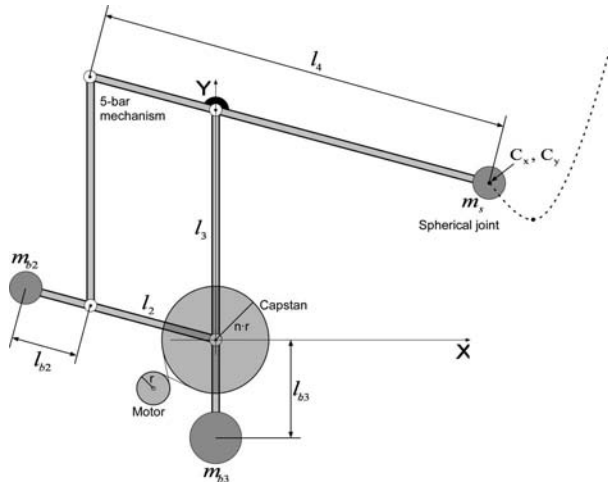

Fig. 2. Schematic view of the balanced 5-dof haptic mechanism, of a random located typical path to follow, and the unknown design parameters.

Because of the nature of the surgical operation, the path ABC lies always on the XY plane. Also, because the patient assumes a constant and predetermined position with respect to the vertical, the same applies to the orientation of path ABC. Because of these observations, the relative location of path ABC with respect to the haptic interface base point O can be described by two parameters that locate one of its point with respect to O. We choose the coordinates C_x, C_y of point C in Fig. 2.

The spherical joint center of mass coincides with the intersection of the last three axes. In other words we assume that the spherical joint is an added mass at the end of link l_4 (see Fig. 2). The next assumption is that in order to design a transparent device we have to eliminate the nonzero gravity terms [9]. We do that by adding two balancing weights on the extensions of links 2 and 3 (see Fig. 3). The last observation is that the lengths of links 1 and 3 are equal. The above-mentioned observations result to the following unknown design parameters (see Table II).

TABLE II
UNKNOWN DESIGN PARAMETERS

Parameter	Explanation
l_2	Length of link 2
l_3	Length of link 3
l_4	Length of link 4
C_x	X coordinate of point C
C_y	Y coordinate of point C
m_{b2}	Balancing weight of link 2
m_{b3}	Balancing weight of link 3
l_{b2}	Extension of link 2
l_{b3}	Extension of link 3
n	Transmission ratio

In Fig. 2, m_s is the spherical joint mass and r is the motor shaft radius. These values are known. Next, the objective function f is defined in a multivariable optimization approach.

A. The Objective Function f

Employing a Lagrangian formulation yields the following mechanism equations of motion:

$$\mathbf{M}(\mathbf{q})\ddot{\mathbf{q}} + \mathbf{V}(\mathbf{q},\dot{\mathbf{q}}) + \mathbf{G}(\mathbf{q}) = \boldsymbol{\tau}' + \mathbf{J}^T\mathbf{F}_T \qquad (1)$$

In (1), $\mathbf{M}(\mathbf{q})$ is the mechanism 5×5 mass matrix, $\ddot{\mathbf{q}}$ is the joint accelerations vector, $\mathbf{V}(\mathbf{q},\dot{\mathbf{q}})$ is a vector, which contains the nonlinear velocity terms, and $\mathbf{G}(\mathbf{q})$ is the gravity torques vector. The vector $\boldsymbol{\tau}'$ contains joint input torques while the vector $\mathbf{J}^T\mathbf{F}_T$ resolves the forces and torques applied by the endoscope to the mechanism endpoint, to the five joints. The equation of motion, as seen from the user side and written for its tip motion, follows:

$$\tilde{\mathbf{M}}\mathbf{v} + \tilde{\mathbf{V}} + \tilde{\mathbf{G}} = \mathbf{J}^{-T}\boldsymbol{\tau} + \mathbf{F}_T \qquad (2a)$$

with

$$\begin{aligned}
\tilde{\mathbf{M}} &= \mathbf{J}^{-T}\mathbf{M}\mathbf{J}^{-1} \\
\tilde{\mathbf{V}} &= \mathbf{J}^{-T}\mathbf{V} - \mathbf{J}^{-T}\mathbf{M}\mathbf{J}^{-1}\dot{\mathbf{J}}\mathbf{J}^{-1}\mathbf{v} \\
\tilde{\mathbf{G}} &= \mathbf{J}^{-T}\mathbf{G}
\end{aligned} \qquad (2b)$$

where $\boldsymbol{\tau}$ is the motor torque vector.

We already mentioned that we wish the entire device induced parasitic forces and torques to be minimum. In (2) these are the inertial terms $\tilde{\mathbf{M}}\mathbf{v}$, the nonlinear velocity terms $\tilde{\mathbf{V}}$, and the gravity terms $\tilde{\mathbf{G}}$. According to that, the objective function that has to be minimized could be the norm of the sum of the above terms:

$$f = Norm(\tilde{\mathbf{M}}\mathbf{v} + \tilde{\mathbf{V}} + \tilde{\mathbf{G}}) \qquad (3)$$

We use the norm because the terms of the above sum are vectors. It is also desirable to find the optimum solution not for a specific configuration but along the whole path ABC of Fig. 1. Therefore we divide the path in k segments and we finally use as objective function, that has to be

minimized, the sum of (3) in each path segment.

$$f = \sum_{i=1}^{k} w_i Norm(\tilde{\mathbf{M}}\mathbf{v} + \tilde{\mathbf{V}} + \tilde{\mathbf{G}})_i \qquad (4)$$

where w_i are the appropriate weights in order to weigh the contribution of each segment. Each segment has different contribution because of the nature of the application. In our case we are more interesting on the behavior of the haptic mechanism at the beginning (point A in Fig. 1), and above all at the end (point C in Fig. 1) of the typical path ABC, because at this point the main operation occurs. In addition to the above objective, one has to take into account several conflicting kinematical and implementation constraints.

B. Constraints For The Objective Function f

1) Inequality constraints

An important constraint is that the mechanism must be large enough to follow typical endoscope paths, such as the one shown in Fig. 1. The following inequality pair describes this constraint for all points along the path,

$$(l_3 - l_{4-2}) \quad \sqrt{x(s)^2 + y(s)^2} \quad (l_3 + l_{4-2}), \qquad (5)$$

where $x(s)$, $y(s)$ are the coordinates of the mechanism tip along the path and $l_{4-2} = l_4 - l_2$, see Fig. 2.

The mechanism should be well conditioned at all configurations. It can be shown that the mechanism condition number is optimum when l_{4-2} $\quad l_4 - l_2 = l_1$ $\quad l_3$ and $q_2 - q_1 = \pi / 2$, while it increases when l_{4-2} $\quad l_1$ and $q_2 - q_1$ $\quad \pi / 2$. The above gives us the following constraint,

$$1 - e_1 \quad l_3 / l_{4-2} \quad 1 + e_1 \qquad (6)$$

$$(\pi / 2) - e_2 \quad q_2 - q_1 \quad (\pi / 2) + e_2, \qquad (7)$$

where e_1, e_2 indicates how strictly the constraint is.

It is important that (4) holds more strictly at the end position of the path, point C in Fig.1, where the main operation takes place. This introduces the next constraint,

$$(\pi / 2) - e_3 \quad q_{2,C} - q_{1,C} \quad (\pi / 2) + e_3, \qquad (8)$$

where $e_2 > e_3$ and the subscript in $q_{i,C}$, i=1, 2 denotes the values of angles q_i at point C.
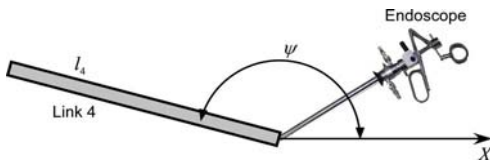

Fig. 3. Angle ψ that is formed by link 4 and the X axis.

Another requirement results from implementation constraints, i.e. to avoid collision between link 4 and the endoscope, the angle $\psi = q_2$ that is formed by link 4 and the X-axis, see Fig. 3, has to be bounded according to

$$1.22\,rad \leq q_2 \leq 5.41\,rad, \qquad (9)$$

which forms another optimization constraint.

During the training procedure, it is possible that the simulator trainees make errors, i.e. they may deviate from the ideal path. In this case, the haptic device must have the capability not only to follow wrong paths, but also to maintain an optimum functionality. In collaboration with specialist surgeons, it was determined that the possible erroneous displacement is about $e = 0.01\,m$ from the typical path. Therefore, it is important to find the optimum location of a whole family of paths that lie around ABC, within the bounds defined by the possible deviation e, and not just of the typical path ABC. This requirement leads to additional constraints.

The mechanism has to follow the perturbed paths,

$$(l_3 - l_{4-2}) \quad \sqrt{x_-(s)^2 + y_-(s)^2} \quad (l_3 + l_{4-2}) \qquad (10)$$

$$(l_3 - l_{4-2}) \quad \sqrt{x_+(s)^2 + y_+(s)^2} \quad (l_3 + l_{4-2}), \qquad (11)$$

where the subscript in $x_-(s)$, $y_-(s)$ and $x_+(s)$, $y_+(s)$ denotes the minimum and maximum perturbation about the ideal path respectively. The mechanism should be well conditioned even in the perturbed path,

$$\begin{aligned} (\pi / 2) - e_4 \quad q_{2+} - q_{1+} \quad (\pi / 2) + e_4 \\ (\pi / 2) - e_5 \quad q_{2-} - q_{1-} \quad (\pi / 2) + e_5 \end{aligned} \qquad (12)$$

where the subscript in $q_{i,+}$, i=1, 2 and $q_{i,-}$, i=1, 2 denotes the values of the angles at the maximum and minimum wrong locations respectively.

The last optimization constraints for the perturbed paths is due to the same implementation constraints as in (9)

$$\begin{aligned} 1.0\,rad \quad q_{2+} \quad 5.585\,rad \\ 1.0\,rad \quad q_{2-} \quad 5.585\,rad \end{aligned} \qquad (13)$$

Equations (5) to (13) form the set of optimization inequality constraints for the objective function f.

2) Equality constraints

In objective function (4) we see that one of the terms is the gravity vector $\tilde{\mathbf{G}} = \mathbf{J}^{-T}\mathbf{G}$ as seen from the user side. We have already mentioned that we could eliminate $\mathbf{G}$ by adding two balancing weights on the extensions of links 2 and 3 (see Fig. 2). It is obvious that if $\mathbf{G}$ is eliminated then $\tilde{\mathbf{G}}$ is also eliminated.

In Table II we see that the balancing weights m_{b2}, m_{b3} and the extensions l_{b2}, l_{b3} are two of the unknown parameters of the optimization procedure. In order to find the values of these parameters that minimize the objective function and at the same time eliminate the gravity vector

G, the optimization procedure selects the values that fulfill the following equality constraints:

$$m_{b2}l_{b2} = m_4 l_{c4} + \sum_{i=5}^{7} m_i l_{4-2} - m_1 l_2 - m_{c2} l_{cb2} - m_2 l_{c2} \quad (14)$$

$$m_{b3}l_{b3} = m_3 l_{c3} + \sum_{i=4}^{7} m_i l_3 - m_{c3} l_{cb3} + m_1 l_{c1} \quad (15)$$

where l_{ci} is the ith link mass center location, m_{ci} is the ith link extension mass and l_{cbi} is the ith link extension mass center location. We notice here that $\sum_{i=5}^{7} m_i = m_s$ is the mass of the three parts that forms the spherical joint and that the spherical joint center of mass coincides with the intersection of the last three axes (see Fig. 2).

Equations (14) and (15) form the set of optimization equality constraints for the objective function f.

IV. OPTIMIZATION RESULTS

For the optimization procedure we used the Matlab optimization toolbox and the function *fmincon*. It is based on a Sequential Quadratic Programming (SQP) method with a few modifications, [15]. It is worth noting that the SQP method is not the only one that solves the optimization problem described here. One could also use other methods, such as the Computational Intelligence and Evolutionary optimization methods [17]. However the aim of this work was to propose a design methodology for haptic mechanisms with special characteristics and not to focus on the particulars of optimization methods.

The function *fmincon* finds a constrained minimum of a function of several variables. The starting guess, the lower and upper bounds are shown in Table III.

TABLE III
STARTING GUESS, LOWER AND UPPER BOUNDS

Parameter	Starting guess	Lower bounds	Upper bounds
Length of link 2, l_2	0.05 m	0.001 m	0.3 m
Length of link 3, l_3	0.05 m	0.001 m	0.3 m
Length of link 4, l_4	0.05 m	0.001 m	0.3 m
X coordinate of point C, C_x	-0.05 m	-0.5 m	0.5 m
Y coordinate of point C, C_y	-0.05 m	-0.5 m	0.5 m
Balanc. weight of link 2, m_{b2}	0.1 Kg	0.0 Kg	0.5 Kg
Balanc. weight of link 3, m_{b3}	0.1 Kg	0.0 Kg	0.5 Kg
Extension of link 2, l_{b2}	0.05 m	-0.3 m	0.3 m
Extension of link 3, l_{b3}	0.05 m	-0.3 m	0.3 m
Transmission ratio, n	5.0	1.0	10.0

The function *fmincon* may only give local solutions. Therefore the optimization search area is divided in several subspaces. The best result of all is chosen as the optimum.

The optimal results are shown in Table IV and

graphically in Fig. 4, where the subscript in $q_{i,s}$, i=1, 2 and $q_{i,e}$, i=1, 2 denotes the values of the angles at the start and the end of the path in the optimum location.

TABLE IV
OPTIMIZATION RESULTS

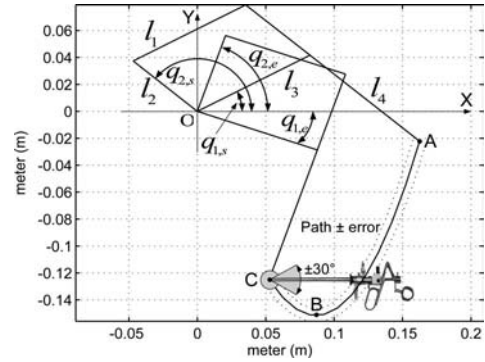| Parameter	Optimization result
Length of link 2, l_2	0.060 m
Length of link 3, l_3	0.093 m
Length of link 4, l_4	0.103 m
X coordinate of point C, C_x	0.053 m
Y coordinate of point C, C_y	-0.124 m
Balancing weight of link 2, m_{b2}	0.080 Kg
Balancing weight of link 3, m_{b3}	0. 241 Kg
Extension of link 2, l_{b2}	0.039 m
Extension of link 3, l_{b3}	0. 052 m
Transmission ratio, n	4.750

Fig. 4. Optimization results.

According to the optimization results all constraints are fulfilled. The mechanism is able to follow the typical path and the possible deviation. Along the typical path shows a small condition number. Fig. 5 shows the condition number and the norm of the parasitic torques of the mechanism along the whole path, which is divided in 12 segments.

Fig. 5 shows that the condition number at the endpoint C of the typical path ABC, a point of great importance where the main operation begins, is very small, $c = 1.12$. At this point we have, $q_2 - q_1 = 1.37\,rad$ and $q_2 = 1.22\,rad$, which are according to the constraints. It is obvious that the second optimization procedure results to better condition number and less parasitic forces.

The pick that we see in Fig. 5 occurs on point B, where the mechanism is stretched out to follow the path, see Fig. 1. It was our choice to give less attention at this point because it is only a pass point through the insertion phase with less importance than points A, where the insertion begins and C, where the main operation phase begins.

It is calculated that the norm of the entire device-induced parasitic forces and torques at point C has a value of 3.1 mNm. The optimization method described in this paper

gives a reduction of the link lengths of about 30% relative to an existing mechanism, see Fig. 6, and 10% relative to the previous optimization procedure described in [16]. Furthermore a reduction to the parasitic forces and torques of about 25% relative to the previous optimization procedure is calculated, see Fig. 5.
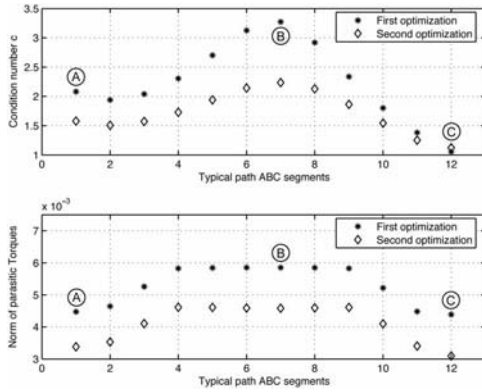

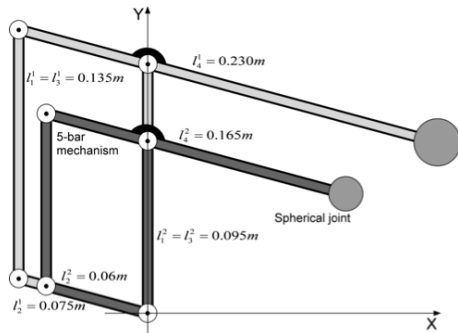Fig. 5. Condition number and norm of the parasitic torques along the typical path ABC.

Fig. 6. Comparison of the initial and new mechanism dimensions.

V. DISCUSSION

The proposed methodology results in a haptic device which is optimum, i.e. its design is the best under the existing constraints. However, in general, there exist three techniques that can maximize the transparency of a haptic device. The first, followed here, is to optimize the design of the devise, the second is to use an appropriate control scheme for compensation of the parasitic terms, and the third is to use both. This work showed that although optimization is needed and must always employed first, it cannot eliminate all devise parasitic forces and torques. To achieve that, a control algorithm is needed to calculate and compensate for them.

In a haptic device, such a control scheme measures the torques/forces applied to the user and compares them to the desired ones, calculated by a mathematical model. The error is fed into an appropriate control algorithm, which sends the command to the motors.

VI. CONCLUSIONS

A design methodology, which aims at the maximization of the transparency for a low-force five-dof haptic device is presented. The haptic device is optimized along a typical path, rather than at some workspace operating point. The minimized objective functions include the entire device induced parasitic forces and torques. The optimization took into account several kinematical and operational constraints that are detailed described. Significant better results are obtained with respect to an existing device.

REFERENCES

[1] Laguna, M. P., Hatzinger, M., and Rassweiler, J., 2002, "Simulators and endourological training," *Current Opinion in Urology 2002*, vol. 12, pp. 209 - 215.
[2] Chen, E., Marcus, B., 1998, "Force Feedback for Surgical Simulation," in *Proceedings of the IEEE*, 86, pp. 524 - 530.
[3] Salisbury, J. K., Srinivasan, A. M., 1997, "Projects in VR. Phantom - Based Haptic Interaction with Virtual Objects," *IEEE Computer Graphics and Applications*, pp. 6 - 10.
[4] D'Aulignac, D., Balaniuk, R., Laugier, C., 2000, "A Haptic Interface for a Virtual Exam of the Human Thigh," in *Proc. IEEE Int. Conference on Robotics and Automation*, pp. 2452 - 2457.
[5] Atsuko, T., Koichi, H., Toyohisa, K., 1998, "Virtual Cutting with Force Feedback," in *Proceedings of the Virtual Reality Annual International Symposium*, pp. 71 - 75.
[6] Baumann, R., et al., 1997, "The PantoScope: A Spherical Remote - Center - of - Motion Parallel Manipulator for Force Reflection," in *Proc. IEEE Int. Conference on Robotics and Automation*, pp. 718 - 723.
[7] Baur, C., Guzzoni, D., Georg, O., 1998, "Virgy, A Virtual Reality and Force Feedback Based Endoscopy Surgery Simulator," in *Proceedings - Medicine Meets Virtual Reality '98*, (MMVR'98), pp. 110 - 116.
[8] Kühnapfel, U., et al., 1997, "The Karlsruhe Endoscopic Surgery Trainer as an example for Virtual Reality in Medical Education," in *Minimally Invasive Therapy and Allied Technologies (MITAT)*, pp. 122-125, Blackwell Science Ltd.
[9] Vlachos, K., Papadopoulos, E., and Mitropoulos, D. N., 2003, "Design and implementation of a haptic device for training in urological operations," *IEEE Transactions on Robotics and Automation*, vol. 19, no. 5, October 2003, pp. 801 - 809.
[10] Khatib, O. and Bowling, A., 1996, "Optimization of the inertial and acceleration characteristics of manipulators," *Proc. IEEE International Conference on Robotics and Automation (ICRA'96)*, Minneapolis, Minnesota, April 1996, vol. 4, pp. 2883-2889.
[11] Stocco, L., Salcudean, S. E., and Sassani, F., 1999, "Fast constrained global optimization of robot parameters," *Robotica*, Vol.16, pp.595-605.
[12] Stocco, L. J., Salcudean, S. E., and Sassani, F., 2001, "Optimal kinematic design of a haptic pen," *IEEE/ASME Transactions on Mechatronics*, vol. 6, no. 3.
[13] Hayward, V., Choksi, J., Lanvin, G., and Ramstein, C., 1994, "Design and multi-objective optimization of a linkage for a haptic interface," *Advances in Robot Kinematics and Computationed Geometry*, A. J. Lenarcic and B. B. Ravani (eds.), Kluwer Academic Publishers, pp. 359 - 368.
[14] Kurtz, R., Hayward, V., 1992, "Multiple-goal kinematic optimization of a parallel spherical mechanism with actuator redundancy," *IEEE Transactions on Robotics and Automation*, vol. 8, no. 5, pp. 644 - 651.
[15] Gill, P.E., W. Murray, and M.H. Wright, Practical Optimization, Academic Press, London, 1981.
[16] Vlachos, K., Papadopoulos, E., and Mitropoulos, D. N., 2004, "Mass/Inertia and Joint Friction Minimization for a Low-force Five-dof Haptic Device," in *Proc. IEEE Int. Conference on Robotics and Automation*, April 26 - May 1, 2004, New Orleans, Louisiana, pp. 286-291.
[17] Th. Bäck and D. B. Fogel, Z.Michalewicz, Handbook of Evolutionary Computation 1&2, Oxford University Press, 1997.